

Acceptor Properties of Boron Subphthalocyanines in Fullerene Free Photovoltaics

Nicola Beaumont,^{†,⊥} Jeffrey S. Castrucci,^{‡,§,⊥} Paul Sullivan,[†] Graham E. Morse,[‡] Andrew S. Paton,[‡] Zheng-Hong Lu,[§] Timothy P. Bender,^{*,‡,§,||} and Tim S. Jones^{*,†}

[†]Department of Chemistry, University of Warwick, Gibbet Hill, Coventry CV4 7AL, U.K.

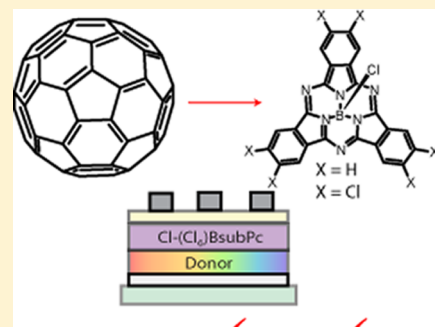
[‡]Department of Chemical Engineering and Applied Chemistry, University of Toronto, 200 College Street, Toronto, Ontario M5S 3E5, Canada

[§]Department of Materials Science and Engineering, University of Toronto, 184 College Street, Toronto, Ontario M5S 3E4, Canada

^{||}Department of Chemistry, University of Toronto, 80 St. George Street, Toronto, Ontario M5S 3H6, Canada

Supporting Information

ABSTRACT: In this paper, we discuss the use of the typical electron-donor (donor) material boron subphthalocyanine chloride (Cl-BsubPc) and a chlorinated derivative (hexachloro boron subphthalocyanine chloride, $\text{Cl}-\text{Cl}_6\text{BsubPc}$) to act as electron-accepting (acceptor) materials and as replacements for C_{60} , when coupled with tetracene and pentacene as the electron-donor materials in organic photovoltaics (OPVs). A large decrease in photocurrent was observed when C_{60} was replaced in the pentacene OPVs, although there was evidence of the harvesting of some triplets for the pentacene/ $\text{Cl}-\text{Cl}_6\text{BsubPc}$ OPV. Large increases in V_{oc} and stability were observed. Photoluminescence quenching, electron mobilities, and photovoltaic device characteristics are also presented and indicate the ambipolar quality of these small molecule organic semiconductors.



1. INTRODUCTION

Small molecule organic photovoltaics (OPVs) have received significant interest over the past few years with power conversion efficiencies now reaching ~12%.¹ In order to further increase efficiencies, new materials,^{2,3} electrodes,⁴ and structures⁵ are being investigated in the hope of competing with existing solar-energy-harvesting technologies while also reducing costs, thus making solar cells economical for the average consumer. A limitation of most small molecule OPV devices is the low spectral coverage in comparison to inorganic photovoltaics. In order to improve power conversion efficiencies, there must be a low spectral overlap between paired materials and preferably absorption into the infrared part of the spectrum to increase solar energy harvesting, which should manifest itself as increased current density from the OPV. Currently, there are a limited number of electron acceptors commonly used within the field of small molecule OPVs, and they are generally fullerene ($\text{C}_{60}/\text{C}_{70}$)-based. A few polymer based acceptors, such as F8TBT (poly((9,9-dioctylfluorene)-2,7-diyl-*alt*-[4,7-bis(3-hexylthien-5-yl)-2,1,3-benzothiadiazole]-2,2diyl)) have shown reasonable performance of ~2%.^{6–8} A number of moieties, including benzothiadiazole and perylene-diimide-based small molecules have been reported, but this work is primarily in bulk heterojunction architectures and paired with standard polymer donors.^{9,10} Recent work has reported efficiencies of ~4%,^{11–13} but these results continue to suffer from low external quantum efficiency (EQE) relative to

analogous soluble fullerene-derivative-based cells, indicating that there is still much opportunity for improvement.

Although C_{60} is a good electron-acceptor material, it is not strongly absorbing and therefore does not contribute largely to the photocurrent. C_{70} has an improved absorption range but is extremely expensive (by ~10 times).^{14,15} High-efficiency single-junction devices also depend on a well-tuned interface gap (I_g = highest occupied molecular orbital_{donor} (HOMO) – lowest unoccupied molecular orbital_{acceptor} (LUMO)) at the heterojunction. C_{60} -based acceptors have low-lying LUMO levels, which drives efficient charge separation but reduces the maximum V_{oc} achieved when paired with oligoacene donors. This difference in LUMO levels (Δ_{LUMO}) between the donor and acceptor is extremely important when suitably matching materials. Despite having similar efficiencies, the open circuit voltage (V_{oc}) in Tc/C_{60} cells is almost double that of pentacene/ C_{60} (0.74 V vs 0.4 V) because of the larger interface gap. Through decreasing the Δ_{LUMO} and increasing the I_g , the achievable V_{oc} will increase, potentially resulting in a larger PCE. Long-term stability is another concern for OPVs, and C_{60} is known to readily photo-oxidize, which results in a gradual reduction in the observed conductivity.¹⁶

Received: April 11, 2014

Revised: June 13, 2014

Published: June 13, 2014



Recently, interest in replacing fullerenes in OPVs has increased, and steady progress is being made to find replacements with equal or improved power conversion efficiencies (PCEs).^{2,3} Phthalocyanines (Pcs) are remarkably stable and strong light-absorbing materials and have thus been identified as suitable candidates for use in OPVs.^{17,18} Boron subphthalocyanines (BsubPc) is a unique form of phthalocyanine and is emerging as a viable class of organic electronic materials with preliminary research into understanding the structure–property relationships between functionalization, solid-state arrangement, and electronic properties recently published.^{19–21} Modified boron subphthalocyanine chlorides have been previously shown to work well as acceptors. Sullivan et al. replaced C_{60} with a peripherally chlorinated boron subphthalocyanine chloride (hexachloro boron subphthalocyanine chloride, Cl–Cl₆BsubPc) alongside a boron subphthalocyanine chloride (Cl-BsubPc) donor and reported a large increase in V_{oc} from 1.10 to 1.31 V for a single-junction all-BsubPc cell.² A perfluorinated analogue synthesized by Gommans et al. increased the V_{oc} in the majority of cases when C_{60} was replaced but, in contrast to the work by Sullivan et al., did not manage to retain a similar PCE.³ Subsequent work using Cl–Cl₆BsubPc as an acceptor paired with a subnaphthalocyanine donor resulted in a significantly elevated PCE.²²

We have previously shown that the Cl-BsubPc²³ and pentafluorophenoxy-BsubPc²⁴ can be used as acceptors, although Cl-BsubPc is more commonly used as a donor material paired with C_{60} .²⁵ By replacing C_{60} with Cl-BsubPc in Tc devices, an increase in short circuit current (J_{sc}), V_{oc} , and PCE is achieved, clearly demonstrating that Cl-BsubPc can also serve as an acceptor.

Oligoacenes, such as tetracene (Tc) and pentacene (Pent) have shown promise for use in organic electronics such as organic thin film transistors (OTFTs) and OPVs because of their optoelectronic properties resulting for their planar fused aromatic ring systems and crystalline bulk structures. Their structural properties allow for high charge-carrier mobilities ($>1\text{ cm}^2\text{ V}^{-1}\text{ s}^{-1}$)²⁶ and relatively long exciton diffusion lengths ($\sim 60\text{ nm}$)²⁷ and have been successfully applied as donor materials in OPVs. Pent and Tc when used in combination with C_{60} can give power conversion efficiencies (η_p , PCE) of $\sim 2\%$.^{23,28–31}

Pent and Tc are also notable for their ability to split one photoexcited singlet state into two triplet states^{32,33} in a process known as singlet fission. The singlet fission process has led to quantum efficiencies exceeding 100% when paired with C_{60} in highly engineered OPV devices.³⁴ The number of known singlet fission capable materials is limited,³⁵ and the number of materials that have been paired with singlet fission capable materials to yield triplet harvesting photovoltaic devices are equally sparse,³⁶ with but a handful of organic semiconductors reported.³⁷ Thus, the desire to identify more pairings of singlet-fission-capable materials with additional triplet dissociating organic acceptors at this point in time is clear.

In this paper, we compare the use of BsubPcs as acceptor materials to C_{60} with reference to the previously published work on Tc/Cl-BsubPc devices. We show that Cl-BsubPc exhibits dual donor/acceptor character by investigating charge mobility through admittance spectroscopy and photoluminescence quenching. Although charge-carrier mobility is identified as a key characteristic in developing new nonfullerene acceptors,³⁸ with a mismatch between donor and acceptor mobilities known to detrimentally impact the fill factor,³⁹ there

are few reports on the charge-carrier mobility of BsubPcs, so we begin to address this shortfall by measuring the electron mobility for both Cl-BsubPc and Cl–Cl₆BsubPc using admittance spectroscopy. We examine the mobility of Cl-BsubPc and Cl–Cl₆BsubPc in light of the long known⁴⁰ and recently confirmed⁴¹ crystal structure of Cl-BsubPc and the crystal structure of Cl–Cl₆BsubPc.⁴² Photovoltaic behavior is exhibited in Pent/BsubPc devices, and we show a large increase in V_{oc} attributed to the increase in I_g of the system. However, a dramatic drop in photocurrent for this pairing is also observed and explained by the relatively poor ability of BsubPcs to harvest triplet energy from Pent compared to C_{60} . That being said, we have observed for the first time the ability of a BsubPc, Cl–Cl₆BsubPc to harvest triplet energy from Pent. In Tc devices, the replacement of C_{60} also results in improved cell stability in air, as indicated by measured device parameters.

2. METHODOLOGY

All OPV samples were grown on commercially available indium tin oxide (ITO)-coated glass substrates (Thin Film Devices, 145 nm thick, $R_s < 15\text{ }\Omega\text{ sq}^{-1}$) after cleaning by sonication in acetone, detergent, water, and isopropanol, and an ultraviolet/ozone treatment decontamination system was used to remove carbon residues (Novascan PSD-UVT).

Photoluminescence (PL) spectroscopy samples were grown on quartz substrates, and PL measurements were taken using a Horiba Yvon with excitation wavelengths 465 nm for Tc samples.

All AFM images were taken using an Asylum Research MFP-3D in tapping mode. MFP-3D software (based on Igor Pro) was used to reconstruct and analyze the images. The images were 5 $\mu\text{m} \times 5\text{ }\mu\text{m}$, and the samples were on ITO substrates (Thin film solids) with a donor layer (pentacene or tetracene) thickness of 60 nm and an acceptor thickness of 5 nm.

Admittance spectroscopy devices were fabricated in a Kurt J. Lesker Luminos cluster tool with a base pressure of $\sim 10^{-8}$ Torr. Cl-BsubPc and Cl–Cl₆BsubPc used for admittance spectroscopy were synthesized by modification of a previously reported method,⁴³ and purified twice using train sublimation⁴⁴ before deposition. The TPBi was purchased from Lumtec and used as received. Organic materials were deposited at a rate of 0.5 \AA/s and metal contacts were deposited at a rate of 1.0 \AA/s in a separate metallization chamber that the sample was transferred to in vacuo. Metal electrodes were deposited through a shadow mask, forming devices with an area of 1 mm \times 2 mm. The sample was transferred through ambient to a vacuum cryostat where impedance spectroscopy measurements were done with an Agilent 4294A Impedance Analyzer and custom LabView software. Film deposition rate was monitored by a quartz crystal monitor, and film thicknesses were measured by the step-edge method using a KLA-Tencor P16+ surface profilometer set to an applied force of 2 mg and a scan speed of 10 $\mu\text{m/s}$.

The OPVs were fabricated using a Kurt. J. Lesker Spectros vacuum evaporation system. The organic materials Tc (Acros, 98%), C_{60} (Nano-C, Inc., 99.5%) were purified using thermal gradient sublimation before deposition, and Cl-BsubPc (Lumtec), bathocuproine (BCP, Aldrich, 96%), and molybdenum oxide (MoO_x , Aldrich, 99.99%) were used as received. The Cl–Cl₆BsubPc was prepared by a previously reported method.² The aluminum electrodes were deposited in situ by evaporation through a shadow mask to a thickness of 100 nm to give an active pixel area of 0.16 cm^2 . Current density–

voltage ($J-V$) characteristics were recorded using a Keithley 2400 sourcemeter with simulated AM 1.5 G solar illumination at 100 mW cm^{-2} (1 sun) from a Newport Oriel solar simulator. External quantum efficiency (EQE) measurements were obtained using a Scientech SF150 xenon arc lamp and a PTI Monochromator. The monochromatic light intensity was calibrated with a Si photodiode (Newport 818-UV) and chopped at 500 Hz. Signal detection was performed with a current–voltage amplifier (Femto DHPGA-100) and lock-in amplifier (Stanford Research SR 830 DSP).

All p -values were calculated using a two tailed z -test. Uncertainties are reported as \pm one standard deviation of the sample mean.

3. RESULTS AND DISCUSSION

The materials used in this study, their respective reported frontier orbital energy levels,^{2,28,45,46} and their respective UV-vis electronic absorption spectra are shown in Figure 1. First, by

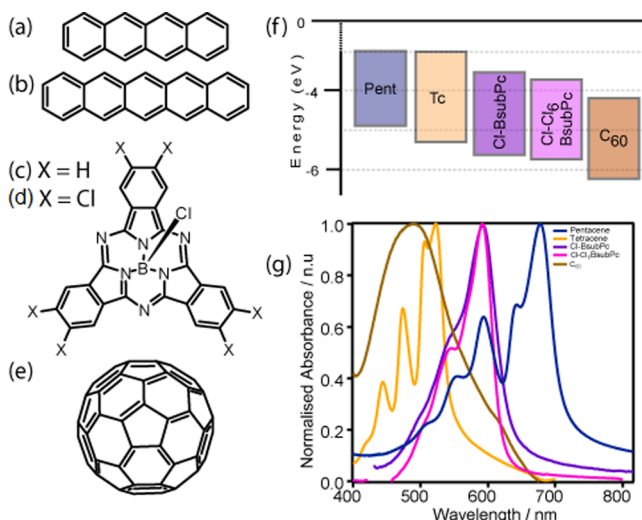


Figure 1. Molecules used within this study: (a) tetracene,²³ (b) pentacene,^{45,46} (c) Cl-BsubPc,²³ (d) Cl-Cl₆BsubPc,² (e) C₆₀,²³ (f) their reported energy levels, and (g) their UV-vis absorption spectra.

considering the energy levels of the Tc/C₆₀ systems (Figure 1f) and by replacing C₆₀ with Cl-Cl₆BsubPc or Cl-BsubPc, there is a corresponding increase in the interface gap from 1.2 to 1.7 eV and to 1.9 eV, respectively. Because of the large increase in I_{sc} for the Tc/Cl-Cl₆BsubPc system, we would expect an increase in V_{oc} for this cell, as seen previously in the Tc/Cl-BsubPc system.²³ A similar increase in V_{oc} is also expected for the Pent/BsubPc devices. In the Tc/Cl-BsubPc system, there is reduced spectral overlap between the donor/acceptor (D/A) Figure 1g), and because the electronic absorption spectrum for the Cl-Cl₆BsubPc is almost unchanged from the underivatized Cl-BsubPc, we would also expect to see photovoltaic behavior resulting with increased J_{sc} relative to the Tc/C₆₀ system for these devices. In the Pent/C₆₀, there is little overlap, but the Pent/BsubPc systems have increased spectral overlap between the donor/acceptor (D/A), and this may result in a decrease in J_{sc} in the Pent/BsubPc devices relative to the Pent/C₆₀ devices.

3.1. Photophysical and Morphological Characterization. The PL quenching of Tc emission by the BsubPcs was investigated with comparison to C₆₀ (Figure 2) to indicate the acceptor character of the BsubPcs. In a vacuum-evaporated bilayer structure (60 nm of Tc and 10 nm of BsubPc), PL

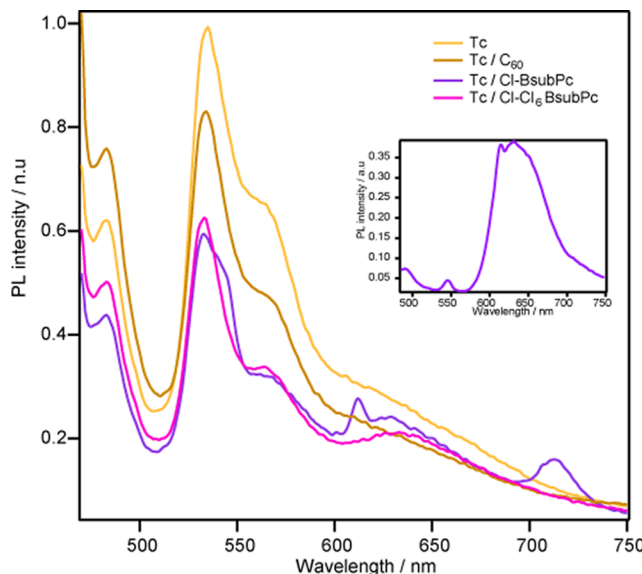


Figure 2. Photoluminescence emission spectra of Tc and Tc/(C₆₀/Cl-BsubPc/Cl-Cl₆BsubPc) bilayers at an excitation wavelength of 465 nm. Inset: PL emission of a 20 nm pristine Cl-BsubPc layer at an excitation of 570 nm.

quenching of \sim 30% of the peak emission at 530 nm is observed from the Tc when using Cl-BsubPc (and Cl-Cl₆BsubPc) as the acceptor whereas C₆₀ (10 nm) quenches \sim 15% of the peak. This effect is not attributed to optical effects, such as a decreased light absorption of the Tc, which would also result in a decrease in emission (discussion shown in the Supporting Information). The peak at \sim 620 nm shows a decrease in PL intensity (\sim 15%) caused by the quenching effect of C₆₀, but there is an increase with the Tc/BsubPc bilayers. This is due to the emission of the BsubPc layer itself, confirmed in the PL spectra for a pristine 20 nm Cl-BsubPc layer (as shown in the inset). This implies that Förster resonant energy transfer (FRET) is also occurring from the Tc to the BsubPcs. FRET is dependent on the overlap of the emission of the donor and the absorption of the acceptor, which is quite substantial in the Tc/BsubPc case. The resultant transfer to the BsubPcs then causes the BsubPc to emit, and this is apparent with the reasonable peak seen at 620 nm. The origin of the additional peak at 720 nm, which is only observed in the Tc/Cl-BsubPc pairing, yet not any of the other pairings, is unclear. We have previously observed aggregate-induced PL and EL emissions from pentafluorophenoxy-BsubPc near 706 nm,^{47,48} but this peak appears to be sufficiently different in wavelength, and conspicuously absent from the neat film PL, to preclude that explanation here.

In order to exclude morphological factors affecting the replacement of C₆₀ bilayer structures were imaged using atomic force microscopy (AFM). Pristine films of Tc and Pent are shown in Figure 3 (T1 and P1) for comparison of the underlying morphology. After the deposition of C₆₀, Cl-BsubPc, and Cl-Cl₆BsubPc onto the acene layers, small features appear on the acene crystallites. Generally, the 5 nm of electron acceptor coats the underlying morphology with a relatively uniform film. The rationale for using a 5 nm acceptor layer was to identify any change in crystallite shape or size of the initial layer near the donor/acceptor interface, as this interface is extremely important to the photovoltaic properties. Once bulk thicknesses >10 nm are reached, the bulk properties of the

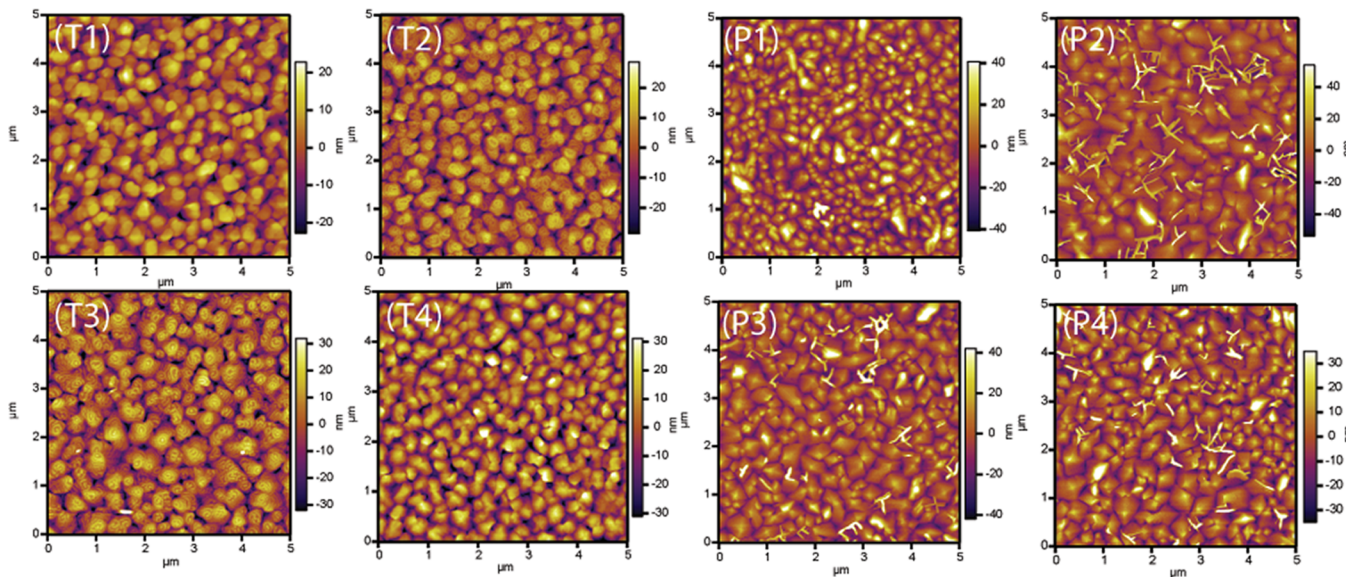


Figure 3. AFM images of semiconductor films and film stacks: (T1) tetracene (T2) Tc/C₆₀ (T3) Tc/Cl-BsubPc and (T4) Tc/Cl-Cl₆BsubPc and (P1) pentacene, (P2) Pent/C₆₀ (P3) Pent/Cl-BsubPc and (P4) Pent/Cl-Cl₆BsubPc.

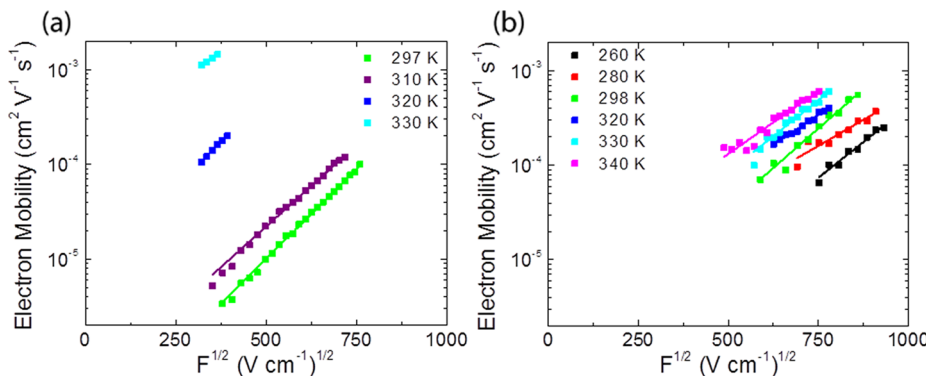


Figure 4. Temperature and field dependence of the electron mobility of (a) Cl-BsubPc and (b) Cl-Cl₆BsubPc.

acceptor layer would dominate the morphology, and it would be difficult to differentiate between the different acceptors at the donor/acceptor interface.

As in previous examples, when a thin film of C₆₀ is deposited on top of an organic layer, small crystallites form across the surface, rather than filling the gaps in between the crystals,^{29,49} and this is also observed when the BsubPcs are deposited on top of the acene layers.⁴⁹ One difference to note between the two acenes is the growth of dendritic crystals in the pentacene films. This is common to all three layers with electron acceptors and is not uncommon in pentacene films. Thin films of pentacene typically reveal large crystallites when grown at 1 Å s⁻¹ and are particularly sensitive to growth rate (faster rates resulting in smaller crystallite size). As seen previously, this deposition rate of growth for pentacene causes the formation of islands with the potential to form large dendritic grains.⁵⁰ This is due to the molecules arriving at the surface with increased opportunity for the strong pentacene–pentacene interactions to overcome any surface interaction. Although this is different to the tetracene layers, the three different electron acceptors appear to deposit in a similar fashion across their respective acenes to each other. Therefore, because of the large influence of the underlying crystalline layers (the morphology of the acenes has a larger influence over device performance), any

change in performance cannot be attributed to the electron-acceptor layer morphology.

3.2. Electrical Device Characterization and Solid-State Arrangements.

Admittance spectroscopy was used to measure the charge transport in BsubPc films. Admittance spectroscopy measures the complex admittance (conductance and capacitance) of a single-carrier device exposed to a small, variable frequency AC perturbation to a DC bias. The dielectric relaxation frequency (f_r) of the film is identified by a peak in the negative differential susceptance ($-\Delta B = 2\pi f(C - C_{geo})$), where f is the AC frequency, C is the frequency dependent capacitance, and C_{geo} is the geometric capacitance). The mobility is then calculated as $\mu = d^2 f_r / (0.56 V)$, where d is the film thickness, and V is the DC bias.⁵¹ The mobility was measured at several temperatures, and all measurements were performed under vacuum in a variable-temperature cryostat.⁵² Electron-only devices with the structure ITO/Al (100 nm)/Cl-BsubPc or Cl-Cl₆BsubPc (200 to 600 nm)/TPBi (3 nm)/Al were used for the impedance spectroscopy measurements where TPBi acts as a buffer layer for protecting BsubPcs from the deposition of aluminum electrodes.⁵³ The temperature and field dependence of the electron mobility of Cl-BsubPc and Cl-Cl₆BsubPc are shown in Figure 4, with the numerical values provided in Table 1 and the Supporting Information.

Table 1. Electron Mobility Parameters^a

acceptor	zero field mobility/cm ² V ⁻¹ s ⁻¹	Poole–Frenkel slope/MV ^{-1/2} cm ^{1/2}	molar density/kmol m ⁻³	motif
Cl-BsubPc	1×10^{-7} (1×10^{-8})	8.8 (0.12)	3.56	concave–concave ribbon
Cl–Cl ₆ BsubPc	8×10^{-7} (2×10^{-7})	7.7 (0.53)	2.72	concave–convex slipped column

^aParameters above are near ambient temperature (standard error from nonlinear curve fit in brackets) for electron-only single-carrier devices analyzed by impedance spectroscopy with a structure ITO/Al (100 nm)/acceptor (200 nm)/TPBi (3 nm)/Al (100 nm) and some crystal structure parameters.

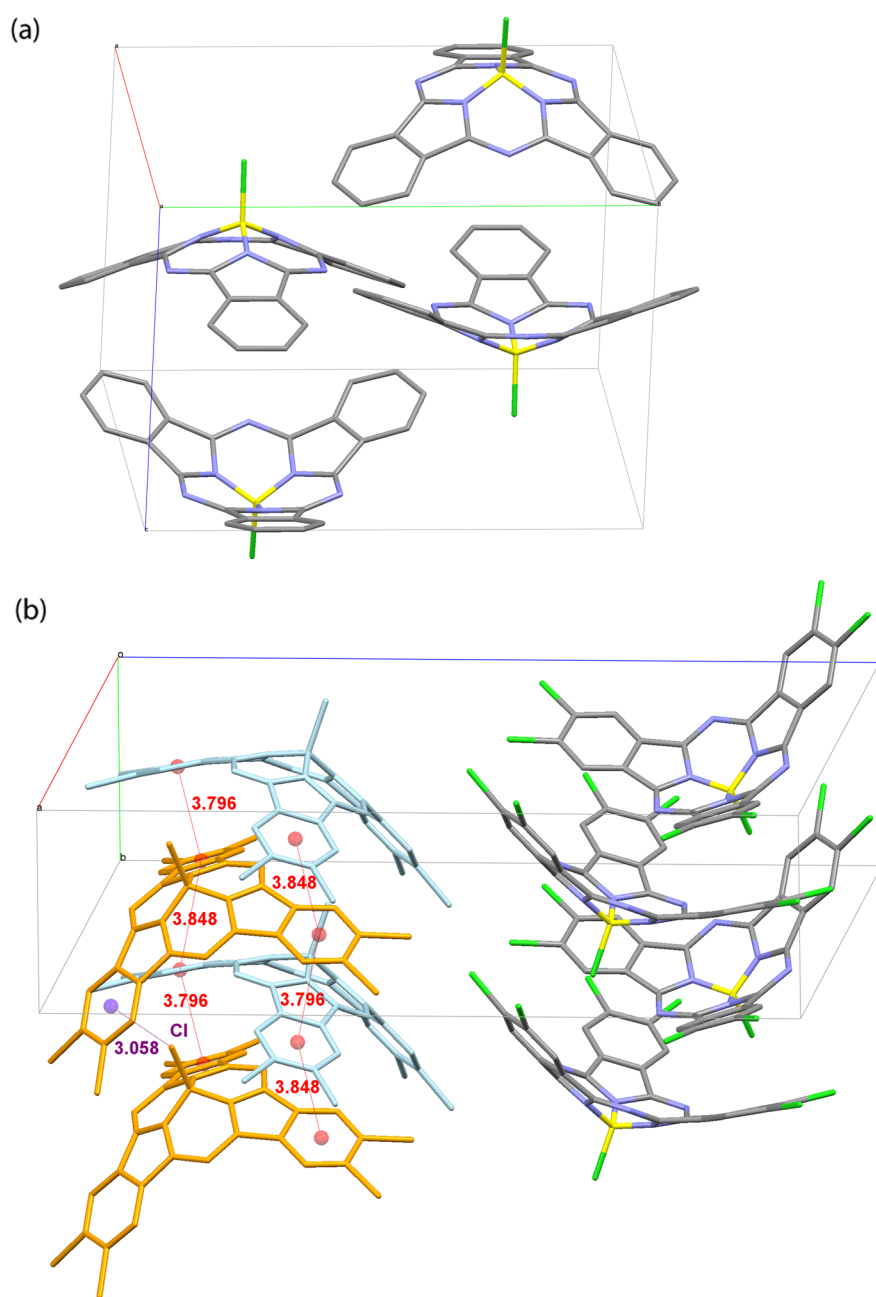


Figure 5. Solid-state arrangement of (a) Cl-BsubPc⁴⁰ and (b) Cl–Cl₆BsubPc.⁴² Hydrogen atoms have been omitted for clarity. Atomic colors: boron – yellow; carbon – gray; nitrogen – blue; chlorine – green. In (b), alternating Cl–Cl₆BsubPc molecules have been colored light blue and orange for clarity; relevant centroids have been colored red.

Reports in the literature of the charge transport properties of BsubPcs are sparse and contradictory. One paper reports mobility within a thin film transistor (TFT) for Cl-BsubPc with the electron and hole mobility $\sim 10^{-5}$ cm² V⁻¹ s⁻¹.⁵⁴ Single-carrier devices are more relevant device architecture to OPVs because charge transport is perpendicular to the substrate in a

single-carrier device as opposed to parallel to the substrate, as is the case in TFTs. Further, organic semiconductors are typically observed to demonstrate a Poole–Frenkel-type (electric-field activated) mobility of the form $\mu(F) = \mu_0 \exp(\gamma F^{1/2})$, where μ_0 is the zero-field mobility, γ is the Poole–Frenkel slope, and F is the electric field. Using single-carrier devices, Poole–Frenkel-

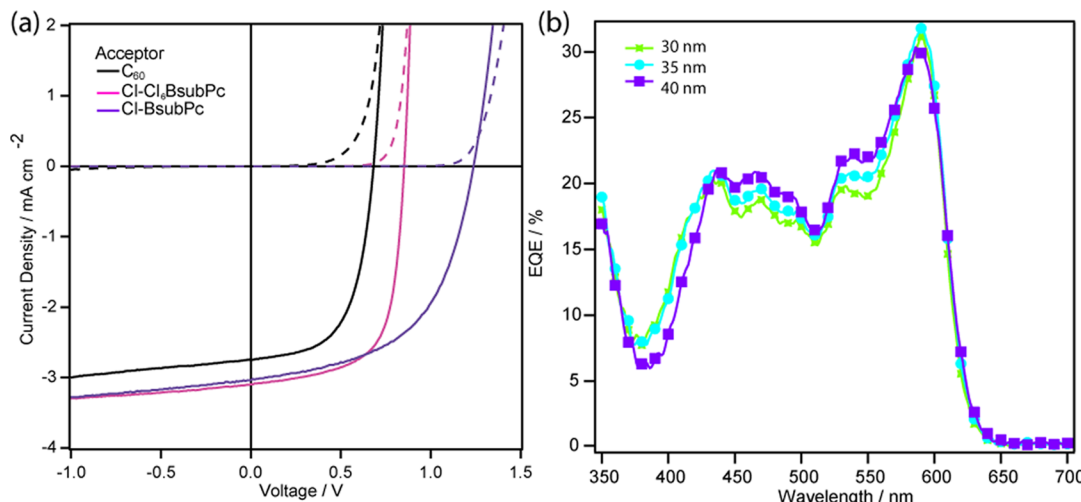


Figure 6. *J*–*V* data under 1 sun illumination for (a) planar Tc heterojunctions and (b) EQE of the Tc/Cl–Cl₆BsubPc device.

type hole mobilities of $\mu_0 = 4.5 \times 10^{-8} \text{ cm}^2 \text{ V}^{-1} \text{ s}^{-1}$, $\gamma = 1.8 \text{ MV}^{-1/2} \text{ cm}^{1/2}$, and electron mobilities of $\mu_0 = 5.2 \times 10^{-10} \text{ cm}^2 \text{ V}^{-1} \text{ s}^{-1}$, $\gamma = 1.2 \text{ MV}^{-1/2} \text{ cm}^{1/2}$ have been measured for BsubPcs.⁵⁵ Then again, it is notoriously difficult to extract reliable mobility measurements from the current/voltage characteristics of single-carrier devices as a result of the confounding of space charge limited current (SCLC) and charge injection limitations, which are also electric-field activated. SCLC analysis of this sort can underestimate mobility by orders of magnitude in the presence of an injection barrier.⁵⁶

Alternative charge-carrier mobility measurement techniques include time-of-flight (TOF) and admittance spectroscopy. Although TOF is a widely used approach for well-established materials, it requires at least 1 μm thick films, which is a disadvantage as it both requires large quantities of material and may not be representative of transport in more device-relevant film thicknesses of less than 100 nm. Conversely, admittance spectroscopy is able to probe much thinner films and is less sensitive to charge-injection limitations at the contacts.⁵¹ There is one study which uses admittance spectroscopy techniques to report an electron mobility of $\sim 10^{-9} \text{ cm}^2 \text{ V}^{-1} \text{ s}^{-1}$ for Cl-BsubPc.⁵⁷ All the reported Cl-BsubPc charge mobilities to date are at ambient temperature and there are no known reports on charge transport in Cl–Cl₆BsubPc. We have previously published an admittance spectroscopy study of electron transport in fluorinated phenoxy boron subphthalocyanines. In that paper, we explored temperature dependence and the impact of solid-state arrangement. The results supported the hypothesis that close packing in different crystal directions could impact zero field mobility and the Poole–Frenkel slope for phenoxy-BsubPcs.²⁰

As with the fluorinated phenoxy BsubPcs, we also considered the temperature activation of the charge-carrier mobility. The thermal activation of Cl-BsubPc electron mobility greatly exceeds the thermal activation of the Cl–Cl₆BsubPc electron mobility with the former showing a change in zero field mobility from $1 \times 10^{-7} \text{ cm}^2 \text{ V}^{-1} \text{ s}^{-1}$ at 297 K to $2 \times 10^{-4} \text{ cm}^2 \text{ V}^{-1} \text{ s}^{-1}$ at 330 K (3 orders of magnitude), although the latter only increases from $8 \times 10^{-7} \text{ cm}^2 \text{ V}^{-1} \text{ s}^{-1}$ to $6 \times 10^{-6} \text{ cm}^2 \text{ V}^{-1} \text{ s}^{-1}$ (1 order of magnitude) over the same temperature range. Application of the Gaussian Disorder Model⁵⁸ to characterize the temperature dependence yielded a poor fit for Cl-BsubPc ($R^2 = 0.86$) and yielded fit parameter values for Cl–Cl₆BsubPc

which had no correlation or meaning in the physical world. Given that the Gaussian Disorder Model was originally developed to describe hopping charge transport between isolated sites in amorphous glasses, the fit to the model may indicate that charge transport in Cl-BsubPc is more similar to transport in an amorphous film, whereas the lack of fit to the model for Cl–Cl₆BsubPc may indicate transport is dominated by more crystalline pathways. Attempts to quantify the charge transport with a band transport model were equally unfruitful, which is unsurprising given band transport is typically only observed when mobilities approach or exceed $1 \text{ cm}^2 \text{ V}^{-1} \text{ s}^{-1}$.⁵⁹ Either way, the similarity in ambient temperature charge-transport values and optical properties for Cl-BsubPc and Cl–Cl₆BsubPc suggests these materials should result in solar cells with similar efficiencies (especially similar optimized device layer thicknesses) if all other device parameters are held constant.

The presence or absence of crystalline transport pathways in Cl–Cl₆BsubPc or Cl-BsubPc can be further supported by considering the solid-state arrangements of each compound as determined by X-ray crystallography of single crystals of each compound (Figure 5). The Cl-BsubPc solid-state arrangement has been long known⁴⁰ and recently confirmed by our group⁴¹ from single crystals grown by train sublimation. Single crystals of Cl–Cl₆BsubPc were grown by acetonitrile–benzene vapor diffusion (CCDC deposition number: 963247).⁴² Each crystal was free of solvent or solvates.

Solid-state interactions (including π – π interaction) between neighboring Cl-BsubPc molecules are practically nonexistent (Figure 5a). There is a minor interaction between C12 and C8 of neighboring molecules at a distance of 3.379 Å (not shown in Figure 5a); however, it is not the geometry that would be indicative of a π – π interaction. Overall, the solid-state arrangement can be described as a ribbon motif permeating through the crystal.

In contrast, the solid-state arrangement of Cl–Cl₆BsubPc shows π – π interactions and forms a columnar assembly (Figure 5b) with concave–convex bowl interactions and interactions less than the sum of the van der Waals radii.⁴² The most relevant interactions are π – π in nature and are between the isoindoline fragments of neighboring Cl₆BsubPc molecules. Two of the three isoindoline units of each Cl–Cl₆BsubPc are associated with two isoindoline units of its neighbor at a

Table 2. Device Parameters Obtained from OPV Devices^a

donor/d _D nm	acceptor/d _A nm	J _{sc} (SD)/mA cm ⁻²	V _{oc} (SD)/V	FF (SD)	η_p (SD)/%	no. of cells tested
A: Tc/60 nm	C ₆₀ /40 nm	2.34 (0.21)	0.67 (0.07)	0.55 (0.08)	0.89 (0.23)	13
B: Tc/60 nm	Cl-BsubPc/35 nm	2.21 (0.25)	1.18 (0.07)	0.53 (0.08)	1.36 (0.24)	11
C: Tc/60 nm	Cl-Cl ₆ BsubPc/35 nm	2.54 (0.32)	0.89 (0.13)	0.50 (0.12)	1.12 (0.31)	17
D: Pent/60 nm	C ₆₀ /40 nm	6.86 (0.48)	0.38 (0.07)	0.53 (0.08)	1.37 (0.35)	50
E: Pent/60 nm	Cl-BsubPc/25 nm	1.35 (0.21)	0.87 (0.10)	0.59 (0.08)	0.65 (0.22)	71
F: Pent/60 nm	Cl-Cl ₆ BsubPc/25 nm	2.09 (0.30)	0.50 (0.02)	0.48 (0.07)	0.50 (0.10)	39

^aDevices A–C have the structure: ITO/MoO_x (5 nm)/Tc (60 nm)/acceptor (d_A nm)/BCP (8 nm)/Al. D–F have the structure: ITO/MoO_x (5 nm)/Pent (60 nm)/acceptor (d_A nm)/BCP (8 nm)/Al. The standard deviation for each characteristic is shown in brackets.

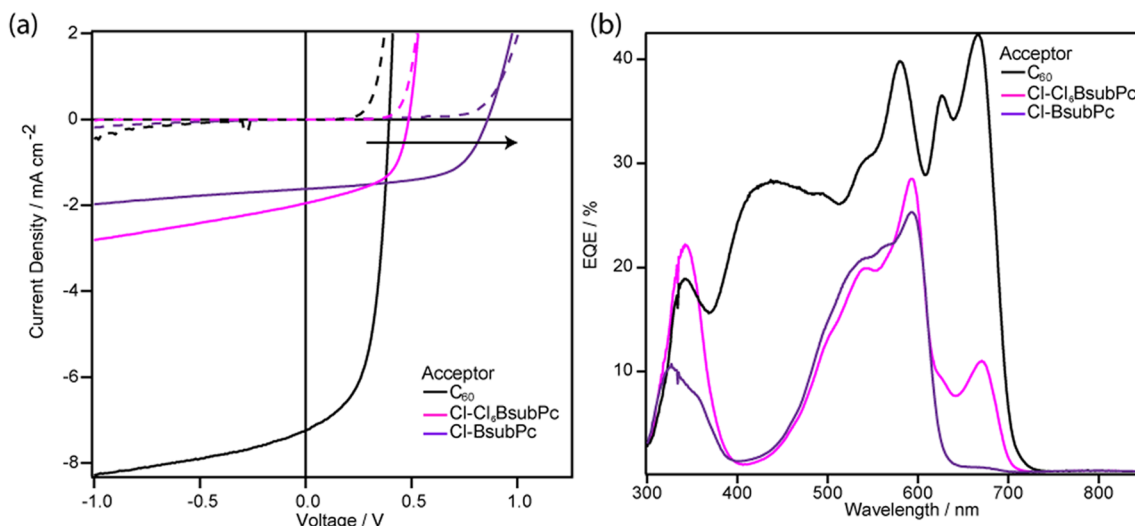


Figure 7. J–V data under 1 sun illumination for (a) planar Pent heterojunctions and (b) EQE of the pentacene devices Pent/C₆₀, Pent/Cl-BsubPc, and Pent/Cl-Cl₆BsubPc with the absorption spectra of a pentacene thin film (red line).

distance less than 4 Å (3.848 and 3.796 Å, Figure 5b), indicating π – π interactions. The third isoindoline unit is involved in a chlorine- π interaction between the axial chloride and the neighboring six-membered outer ring with an interaction distance of 3.058 Å (Figure 5b). These three dominant intermolecular interactions drive the formation of what resembles a slip-stacked columnar arrangement of columns throughout the crystal structure of Cl-Cl₆BsubPc. The presence of such strong interactions in the solid state lends itself to the idea that Cl-Cl₆BsubPc might be more crystalline in the bulk than Cl-BsubPc.

3.3. Photovoltaic Device Characterization. In order to probe the effect of replacing C₆₀ with the BsubPcs, we fabricated bilayer heterojunction OPVs comprising of ITO/MoO_x (5 nm)/Tc or Pent (60 nm)/acceptor (d_A nm)/BCP (8 nm)/Al. The insertion of the 5 nm MoO_x interlayer allows for improved energy level alignment at the electrode/Tc interface and was used in the Pent devices to allow for consistency but has no effect on cell performance, as shown previously.⁴ Current density versus voltage characteristics in the dark and under 1 sun illumination (AM 1.5G) for these cells are shown in Figure 6 with key device parameters listed in Table 2.

Figure 6a shows the device characteristics for the replacement of C₆₀ with BsubPcs in Tc-based devices. As expected, the replacement of C₆₀ with Cl-Cl₆BsubPc yielded an increase in both V_{oc} to 0.89 ± 0.13 V ($p = 2.8 \times 10^{-9}$) and J_{sc} to 2.54 ± 0.32 mA cm⁻² ($p = 0.039$), and the resulting PCE is improved by 50% ($p = 0.019$). When compared with the two reference devices, the V_{oc} falls between the Tc/C₆₀ and Tc/Cl-BsubPc devices (due to the I_g falling between these two

extremes), whereas the short circuit current is unchanged from the Tc/Cl-BsubPc cell ($p = 0.17$). The fill factors are also identical between the Cl-BsubPc and Cl-Cl₆BsubPc devices ($p = 0.43$). Both these similarities are attributed to similar quenching abilities, electron mobilities, and efficient exciton dissociation. Cl-Cl₆BsubPc also contributes to the photocurrent in the external quantum efficiency similar to the Tc/Cl-BsubPc devices published previously, as shown in Figure 6b.

Current density versus voltage characteristics of the Pent devices are shown in Figure 7 with the corresponding parameters also in Table 2. The optimal Pent thickness when paired with 40 nm C₆₀ is ~60 nm, with a J_{sc} of 6.86 ± 0.48 mA cm⁻², a V_{oc} of 0.38 ± 0.07 V, and a FF and η_p of 0.53 ± 0.08 and $1.37 \pm 0.35\%$, respectively, which is similar to previous literature.²⁹ In the previous case of Tc/Cl-BsubPc, there was no increase in J_{sc} due to the reduced spectral overlap in comparison to Tc/C₆₀, but in this case, the Pent/BsubPc pairing overlap greatly at the 595 nm absorption peak of BsubPc, and therefore, a small decrease in J_{sc} was expected. However, there is a loss of ~5 mA cm⁻² for both BsubPcs, leading to Cl-BsubPc and Cl-Cl₆BsubPc devices having lower J_{sc} of 1.35 ± 0.21 mA cm⁻² ($p < 10^{-200}$) and 2.09 ± 0.30 mA cm⁻² ($p < 10^{-200}$). Fill factor is largely unchanged between Cl-BsubPc and Cl-Cl₆BsubPc in the Tc system with 0.53 ± 0.08 versus 0.50 ± 0.12 ($p = 0.43$), whereas in the Pent system, the fill factors differ, with 0.59 ± 0.08 versus 0.48 ± 0.07 ($p = 4.86 \times 10^{-5}$). The optimized acceptor layer thickness in Tc-containing cells is the same (35 nm) for both Cl-BsubPc and Cl-Cl₆BsubPc, and the same holds for the optimized acceptor layer thickness (25 nm) in Pent-containing cells. This

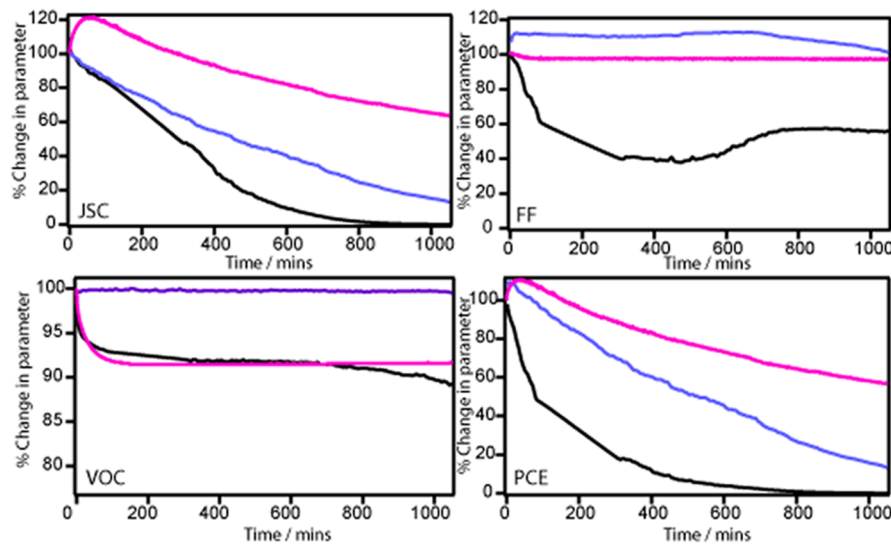


Figure 8. Device parameters of Tc/C_{60} (black); $\text{Tc}/\text{Cl}-\text{BsubPc}$ (purple); $\text{Tc}/\text{Cl}-\text{Cl}_6\text{BsubPc}$ (pink) cells under constant illumination over 23.2 h in air.

highlights how an understanding of charge transport can be useful in device design even if it is not the only relevant material parameter, as emphasized by the dramatic drop in J_{sc} for the Pent-containing devices. It seems apparent that there must be another cause for the dramatic loss of photocurrent.

In an effort to better understand the dramatic decrease in J_{sc} the external quantum efficiency (EQE) of the Pent/BsubPc OPV cells are shown in Figure 7b. Although we would expect to see the Pent contribution between 500–700 nm (as shown in the absorption spectra, Figure 1g), the only dominant peak present is at 595 nm, a wavelength associated with BsubPc absorption. This is in contrast with some other pentacene/nonfullerene acceptor cells where pentacene has been the dominant contributor to photocurrent.⁶⁰ The current would be reduced because of the overlap in absorption spectra, but we would expect more of a contribution from the Pent layer, particularly at wavelengths longer than 600 nm. The Tc/C_{60} cell is known to benefit from enhanced photocurrent due to triplet fission,^{32,36,37} so we propose that the dramatic loss of photocurrent in the Pent/BsubPc cells is a result of the interface poorly dissociating these pentacene-originating triplets. (There are few measurements of triplet energies in BsubPcs, but an estimate of 1.45 eV for a related derivative,⁶¹ in contrast to Pent's triplet energy, recently bounded between 0.85 and 1.00 eV,³⁶ suggests that triplets generated in the Pent layer would not transfer to the BsubPc layer.) The small EQE peak at 670 nm in the $\text{Tc}/\text{Cl}-\text{Cl}_6\text{BsubPc}$ cell that is completely absent in the $\text{Tc}/\text{Cl}-\text{BsubPc}$ cell is a dominant feature in the Tc/C_{60} cell. We thus interpret these results to indicate that Cl-BsubPc does not facilitate the dissociation of Pent triplets, but Cl-Cl₆BsubPc does dissociate some Pent-derived triplets, albeit not as efficiently as C₆₀. This is the first report of a BsubPc-facilitating triplet harvesting from Pent. Following the reasoning of Ehrler et al.³⁶ we would propose that a BsubPc derivative with a deeper LUMO energy would likely be an even more effective at harvesting Pent-derived triplets, resulting in enhanced photocurrent. Similar observations were not made in the Tc-containing OPVs as a pair of triplets in Tc are essentially degenerate with the singlet energy,⁶² so the triplet generation process is orders of magnitude slower in Tc³³ than in Pent.³²

We previously demonstrated improved cell stability with the replacement of C₆₀ with Cl-Cl₆BsubPc in BsubPc (as the donor) OPVs. A large improvement in cell stability toward air (and N₂) was achieved when tested under constant illumination of 100 mW cm⁻² AM1.5G for 60 min.² To investigate the stability of the electron-accepting materials, a summary of the degradation of PV parameters over 1100 min of constant AM 1.5G illumination in air are shown in Figure 8. Twelve devices per structure were tested simultaneously, and representative device performance is shown in the figure. The cells studied have the structure: ITO/MoO_x/Tc/Acceptor/BCP/Al and were tested in air. Tc was chosen as the electron-donor material due to both layers contributing to the photocurrent, although similar trends were observed in the Pent OPVs. In all cases, the cells degrade, the most dramatic of which is the Tc/C_{60} device. The main decrease is due to a fast degradation in J_{sc} and FF presumably caused by the oxidation of C₆₀ (in air) resulting in a decrease in conductivity. When replacing the acceptor layer with BsubPc, the cells are more stable than their C₆₀ counterparts in all parameters and still retain 20% of the original efficiency at ~1000 min (compared to 0% at 800 min with Tc/C_{60}). The Tc/BsubPc cell shows no change in V_{oc} over the measurement time, and the main cause of the degradation is the decrease in J_{sc} . The $\text{Tc}/\text{Cl}-\text{Cl}_6\text{BsubPc}$ device is the most stable over the time frame, losing only 40% of its efficiency. We attribute the unusual initial rise in the J_{sc} of the $\text{Tc}/\text{Cl}-\text{Cl}_6\text{BsubPc}$ cells and the FF of the $\text{Tc}/\text{Cl}-\text{BsubPc}$ cells to be a possible thermal effect as the cells reach an equilibrium temperature in our testing station. The FF is extremely stable, with most of the change in PCE the result of the sharp initial reduction in V_{oc} and the steady decrease in the J_{sc} . The chlorinated derivative is likely to be more stable than Cl-BsubPc as a result of the lower ionization potential and has been seen previously for halogenated derivatives.^{63,64} Although the degradation of the photocurrent is slower than the other systems, it still shows the poor stability of these small molecules in air. As the decrease in J_{sc} occurs in all systems, it is probably partly down to the Tc layer, with the [4 + 2] cycloaddition with singlet oxygen the main degradation pathway rendering it colorless over time.⁶⁵ This consistent degradation highlights the further need for good encapsulants, because although the

stability can be improved with simple modifications, like the replacement of fullerenes, O₂ infiltration and moisture remains a problem.

4. CONCLUSION

In summary, we have demonstrated that the archetypal donor material Cl-BsubPc has ambipolar characteristics both when derivatized (Cl—Cl₆BsubPc) and underivatized (Cl-BsubPc), showing reasonable electron mobility and photoluminescence quenching of excitons from Tc films. When incorporated in devices as the acceptor material, the voltage can be dramatically increased both in Tc- and Pent-containing devices, and this large improvement in V_{oc} was observed as a result of the increase in interface gap. The similarity in room temperature electron mobility of Cl-BsubPc and Cl—Cl₆BsubPc may explain why devices with each material were found to have the same optimal acceptor thicknesses. The device stability can also be improved on the replacement of C₆₀ in nearly all cases and highlights another advantage for using BsubPcs. This dual donor/acceptor character for BsubPc semiconductors allows for an increased assortment of materials for the future design of high-voltage and singlet-fission harvesting devices. This work also highlights the need for optimizing energetics and measuring charge-carrier mobility in devices to identify new material development targets and ultimately achieve higher efficiencies.

■ ASSOCIATED CONTENT

Supporting Information

The photoluminescence discussion, tabular information on the temperature dependent and field-dependent mobility parameters for the materials, statistical analysis, and detailed crystallographic data for Cl—Cl₆BsubPc are given in the Supporting Information. This material is available free of charge via the Internet at <http://pubs.acs.org>.

■ AUTHOR INFORMATION

Corresponding Authors

*E-mail: tim.bender@utoronto.ca.
*E-mail: t.s.jones@warwick.ac.uk.

Author Contributions

[†]The manuscript was written through contributions of all authors. All authors have given approval to the final version of the manuscript. N.B. and J.S.C. contributed equally.

Notes

The authors declare no competing financial interest.

■ ACKNOWLEDGMENTS

This work was supported by the Engineering and Physical Sciences Research Council [Grant Number EP/G031088/1]. This work was supported by a Natural Sciences and Engineering Research Council (NSERC) Post Graduate Scholarships (Doctoral Level) to JSC and GEM and a Discovery Grant to TPB. We also acknowledge Khalveer Chall and Prof. Mike Shipman for the synthesis of Cl—Cl₆BsubPc at the University of Warwick and Dr. Thomas Howells for use of the optical model.

■ REFERENCES

- (1) Heliatek Consolidates Its Technology Leadership by Establishing a New World Record for Organic Solar Technology with a Cell Efficiency of 12%. <http://www.heliatek.com/wp-content/uploads/>

2013/01/130116_PR_Heliatek_achieves_record_cell_efficiency_for_OPV.pdf (accessed May 29 2013).

(2) Sullivan, P.; Duraud, A.; Hancox, I.; Beaumont, N.; Mirri, G.; Tucker, J. H. R.; Hatton, R. A.; Shipman, M.; Jones, T. S. Halogenated Boron Subphthalocyanines as Light Harvesting Electron Acceptors in Organic Photovoltaics. *Adv. Energy Mater.* **2011**, *1*, 352–355.

(3) Gommans, H.; Aernouts, T.; Verreet, B.; Heremans, P.; Medina, A.; Claessens, C. G.; Torres, T. Perfluorinated Subphthalocyanine as a New Acceptor Material in a Small-Molecule Bilayer Organic Solar Cell. *Adv. Funct. Mater.* **2009**, *19*, 3435–3439.

(4) Hancox, I.; Sullivan, P.; Chauhan, K. V.; Beaumont, N.; Rochford, L. A.; Hatton, R. A.; Jones, T. S. The Effect of a MoO_x Hole-Extracting Layer on the Performance of Organic Photovoltaic Cells Based on Small Molecule Planar Heterojunctions. *Org. Electron.* **2010**, *11*, 2019–2025.

(5) Riede, M.; et al. Efficient Organic Tandem Solar Cells Based on Small Molecules. *Adv. Funct. Mater.* **2011**, *21*, 3019–3028.

(6) Hodgkiss, J. M.; Albert-Seifried, S.; Rao, A.; Barker, A. J.; Campbell, A. R.; Marsh, R. A.; Friend, R. H. Exciton-Charge Annihilation in Organic Semiconductor Films. *Adv. Funct. Mater.* **2012**, *22*, 1567–1577.

(7) McNeill, C. R.; Abrusci, A.; Zaumseil, J.; Wilson, R.; McKiernan, M. J.; Burroughes, J. H.; Halls, J. J. M.; Greenham, N. C.; Friend, R. H. Dual Electron Donor/Electron Acceptor Character of a Conjugated Polymer in Efficient Photovoltaic Diodes. *Appl. Phys. Lett.* **2007**, *90*, 193506.

(8) McNeill, C. R.; Greenham, N. C. Charge Transport Dynamics of Polymer Solar Cells under Operating Conditions: Influence of Trap Filling. *Appl. Phys. Lett.* **2008**, *93*, 203310.

(9) Bloking, J. T.; et al. Solution-Processed Organic Solar Cells with Power Conversion Efficiencies of 2.5% Using Benzothiadiazole/Imide-Based Acceptors. *Chem. Mater.* **2011**, *23*, 5484–5490.

(10) Schwenn, P. E.; et al. A Small Molecule Non-Fullerene Electron Acceptor for Organic Solar Cells. *Adv. Energy Mater.* **2011**, *1*, 73–81.

(11) Bloking, J. T.; Giovenzana, T.; Higgs, A. T.; Ponec, A. J.; Hoke, E. T.; Vandewal, K.; Ko, S.; Bao, Z.; Sellinger, A.; McGehee, M. D. Comparing the Device Physics and Morphology of Polymer Solar Cells Employing Fullerenes and Non-Fullerene Acceptors. *Adv. Energy Mater.* **2014**, DOI: 10.1002/aenm.201301426.

(12) Lin, Y.; Wang, J.; Dai, S.; Li, Y.; Zhu, D.; Zhan, X. A Twisted Dimeric Perylene Diimide Electron Acceptor for Efficient Organic Solar Cells. *Adv. Energy Mater.* **2014**, DOI: 10.1002/aenm.201400420.

(13) Lu, Z.; Jiang, B.; Zhang, X.; Tang, A.; Chen, L.; Zhan, C.; Yao, J. Perylene-Diimide Based Non-Fullerene Solar Cells with 4.34% Efficiency through Engineering Surface Donor/Acceptor Compositions. *Chem. Mater.* **2014**, *26*, 2907–2914.

(14) TermUSA. Fullerene Pricing. <http://www.fullerenesforsale.com/price.html> (accessed May 29 2013).

(15) SESResearch. Buy Fullerene. <https://sesres.com/Fullerene.asp> (accessed May 29 2013).

(16) Asakawa, T.; Sasaki, M.; Shiraishi, T.; Koinuma, K. Dark and Photoconductivity Behaviors of Amorphous and Crystalline C₆₀ Films. *Jpn. J. Appl. Phys., Part 1* **1995**, *34*, 1958–1962.

(17) Wohrle, D.; Schulte, B. Polymeric Phthalocyanines and Their Precursors 0.10. Thermal-Stability of Polymeric Phthalocyanines and Their Low-Molecular Analogs. *Makromol. Chem.* **1985**, *186*, 2229–2245.

(18) Stefani, V.; Cabezon, B.; Denardin, E. L. G.; Samios, D.; Torres, T. Triazolephthalocyanine Versus Phthalocyanine Nickel(II) and Copper(II) Complexes: A Thermogravimetric Stability Study. *J. Mater. Chem.* **2000**, *10*, 2187–2192.

(19) Morse, G. E.; Castrucci, J. S.; Helander, M. G.; Lu, Z. H.; Bender, T. P. Phthalimidoboronsubphthalocyanines: New Derivatives of Boronsubphthalocyanine with Bipolar Electrochemistry and Functionality in OLEDs. *ACS Appl. Mater. Interfaces* **2011**, *3*, 3538–3544.

(20) Castrucci, J. S.; Helander, M. G.; Morse, G. E.; Lu, Z. H.; Yip, C. M.; Bender, T. P. Charge Carrier Mobility in Fluorinated Phenoxy

- Boron Subphthalocyanines: Role of Solid State Packing. *Cryst. Growth Des.* **2012**, *12*, 1095–1100.
- (21) Morse, G. E.; Bender, T. P. Boron Subphthalocyanines as Organic Electronic Materials. *ACS Appl. Mater. Interfaces* **2012**, *4*, 5055–5068.
- (22) Verreet, B.; Cnops, K.; Cheyns, D.; Heremans, P.; Stesmans, A.; Zango, G.; Claessens, C. G.; Torres, T.; Rand, B. P. Decreased Recombination through the Use of a Non-Fullerene Acceptor in a 6.4% Efficient Organic Planar Heterojunction Solar Cell. *Adv. Energy Mater.* **2014**, DOI: 10.1002/aenm.201301413.
- (23) Beaumont, N.; Cho, S. W.; Sullivan, P.; Newby, D.; Smith, K. E.; Jones, T. S. Boron Subphthalocyanine Chloride as an Electron Acceptor for High-Voltage Fullerene-Free Organic Photovoltaics. *Adv. Funct. Mater.* **2012**, *22*, 561–566.
- (24) Morse, G. E.; Gantz, J. L.; Steirer, K. X.; Armstrong, N. R.; Bender, T. P. Pentafluorophenoxy Boron Subphthalocyanine (FSbsubpc) as a Multifunctional Material for Organic Photovoltaics. *ACS Appl. Mater. Interfaces* **2014**, *6*, 1515–24.
- (25) Mutolo, K. L.; Mayo, E. I.; Rand, B. P.; Forrest, S. R.; Thompson, M. E. Enhanced Open-Circuit Voltage in Subphthalocyanine/C₆₀ Organic Photovoltaic Cells. *J. Am. Chem. Soc.* **2006**, *128*, 8108–8109.
- (26) Anthony, J. E. The Larger Acenes: Versatile Organic Semiconductors. *Angew. Chem., Int. Ed.* **2008**, *47*, 452–483.
- (27) Yoo, S.; Domercq, B.; Kippelen, B. Efficient Thin-Film Organic Solar Cells Based on Pentacene/C-60 Heterojunctions. *Appl. Phys. Lett.* **2004**, *85*, 5427–5429.
- (28) Yoo, S.; et al. Analysis of Improved Photovoltaic Properties of Pentacene/C-60 Organic Solar Cells: Effects of Exciton Blocking Layer Thickness and Thermal Annealing. *Solid-State Electron.* **2007**, *51*, 1367–1375.
- (29) Sullivan, P.; Jones, T. S. Pentacene/Fullerene (C₆₀) Heterojunction Solar Cells: Device Performance and Degradation Mechanisms. *Org. Electron.* **2008**, *9*, 656–660.
- (30) Chu, C. W.; Shao, Y.; Shrotriya, V.; Yang, Y. Efficient Photovoltaic Energy Conversion in Tetracene-C₆₀ Based Heterojunctions. *Appl. Phys. Lett.* **2005**, *86*, 243506.
- (31) Beaumont, N.; Hancox, I.; Sullivan, P.; Hatton, R. A.; Jones, T. S. Increased Efficiency in Small Molecule Organic Photovoltaic Cells through Electrode Modification with Self-Assembled Monolayers. *Energy Environ. Sci.* **2011**, *4*, 1708–1711.
- (32) Rao, A.; Wilson, M. W. B.; Hodgkiss, J. M.; Albert-Seifried, S.; Bassler, H.; Friend, R. H. Exciton Fission and Charge Generation Via Triplet Excitons in Pentacene/C₆₀ Bilayers. *J. Am. Chem. Soc.* **2010**, *132*, 12698–12703.
- (33) Smith, M. B.; Michl, J. Singlet Fission. *Chem. Rev.* **2010**, *110*, 6891–6936.
- (34) Congreve, D. N.; Lee, J.; Thompson, N. J.; Hontz, E.; Yost, S. R.; Reusswig, P. D.; Bahlke, M. E.; Reineke, S.; Van Voorhis, T.; Baldo, M. A. External Quantum Efficiency above 100% in a Singlet-Exciton-Fission-Based Organic Photovoltaic Cell. *Science* **2013**, *340*, 334–337.
- (35) Smith, M. B.; Michl, J. Recent Advances in Singlet Fission. *Annu. Rev. Phys. Chem.* **2013**, *64*, 361–386.
- (36) Ehrler, B.; Walker, B. J.; Bohm, M. L.; Wilson, M. W.; Vaynzof, Y.; Friend, R. H.; Greenham, N. C. In Situ Measurement of Exciton Energy in Hybrid Singlet-Fission Solar Cells. *Nat. Commun.* **2012**, *3* (1019), 1–6.
- (37) Jadhav, P. J.; et al. Triplet Exciton Dissociation in Singlet Exciton Fission Photovoltaics. *Adv. Mater.* **2012**, *24*, 6169–6174.
- (38) Anthony, J. E. Small-Molecule, Nonfullerene Acceptors for Polymer Bulk Heterojunction Organic Photovoltaics. *Chem. Mater.* **2011**, *23*, 583–590.
- (39) Tress, W.; Petrich, A.; Hummert, M.; Hein, M.; Leo, K.; Riede, M. Imbalanced Mobilities Causing S-Shaped IV Curves in Planar Heterojunction Organic Solar Cells. *Appl. Phys. Lett.* **2011**, *98*, 063301.
- (40) Kietabl, H. Die Kristall- Und Molekülstruktur Eines Neuartigen Phthalocyaninähnlichen Borkomplexes. *Monatshefte für Chemie* **1974**, *105*, 405–418.
- (41) Fulford, M. V.; Jaidka, D.; Paton, A. S.; Morse, G. E.; Brisson, E. R. L.; Lough, A. J.; Bender, T. P. Crystal Structures, Reaction Rates, and Selected Physical Properties of Halo-Boron-subphthalocyanines (Halo = Fluoride, Chloride, and Bromide). *J. Chem. Eng. Data* **2012**, *57*, 2756–2765.
- (42) Morse, G. E.; Gong, I.; Kawar, Y.; Lough, A. J.; Bender, T. P. Crystal and Solid State Arrangement Trends of Halogenated Boron Subphthalocyanines. *Cryst. Growth Des.* **2014**, *14*, 2138–2147.
- (43) Zyskowski, C. D.; Kennedy, V. O. Compounds in the Series from Boron Subphthalocyanine to Boron Subnaphthalocyanine. *J. Porphyrins Phthalocyanines* **2000**, *4*, 707–712.
- (44) Wagner, H. J.; Loutfy, R. O.; Hsiao, C. K. Purification and Characterization of Phthalocyanines. *J. Mater. Sci.* **1982**, *17*, 2781–2791.
- (45) Watkins, N. J.; Gao, Y. Interface Formation and Energy Level Alignment of Pentacene on SiO₂. *J. Appl. Phys.* **2003**, *94*, 5782–5786.
- (46) Schroeder, P. G.; France, C. B.; Park, J. B.; Parkinson, B. A. Energy Level Alignment and Two-Dimensional Structure of Pentacene on Au(111) Surfaces. *J. Appl. Phys.* **2002**, *91*, 3010–3014.
- (47) Morse, G. E.; Helander, M. G.; Maka, J. F.; Lu, Z.-H.; Bender, T. P. Fluorinated Phenoxy Boron Subphthalocyanines in Organic Light-Emitting Diodes. *ACS Appl. Mater. Interfaces* **2010**, *2*, 1934–1944.
- (48) Helander, M. G.; Morse, G. E.; Qiu, J.; Castrucci, J. S.; Bender, T. P.; Lu, Z. H. Pentafluorophenoxy Boron Subphthalocyanine as a Fluorescent Dopant Emitter in Organic Light Emitting Diodes. *ACS Appl. Mater. Interfaces* **2010**, *2*, 3147–3152.
- (49) Cnops, K.; Rand, B. P.; Cheyns, D.; Heremans, P. Enhanced Photocurrent and Open-Circuit Voltage in a 3-Layer Cascade Organic Solar Cell. *Appl. Phys. Lett.* **2012**, *101*, 143301.
- (50) Potsavage, W. J.; Sharma, A.; Kippelen, B. Critical Interfaces in Organic Solar Cells and Their Influence on the Open-Circuit Voltage. *Acc. Chem. Res.* **2009**, *42*, 1758–1767.
- (51) Tsang, S. W.; So, S. K.; Xu, J. B. Application of Admittance Spectroscopy to Evaluate Carrier Mobility in Organic Charge Transport Materials. *J. Appl. Phys.* **2006**, *99*, 013706.
- (52) Helander, M. G.; Wang, Z. B.; Greiner, M. T.; Qiu, J.; Lu, Z. H. Experimental Design for the Determination of the Injection Barrier Height at Metal/Organic Interfaces Using Temperature Dependent Current-Voltage Measurements. *Rev. Sci. Instrum.* **2009**, *80*, 033901.
- (53) Morse, G. E.; Helander, M. G.; Maka, J. F.; Lu, Z. H.; Bender, T. P. Fluorinated Phenoxy Boron Subphthalocyanines in Organic Light-Emitting Diodes. *ACS Appl. Mater. Interfaces* **2010**, *2*, 1934–1944.
- (54) Yasuda, T.; Tsutsui, T. N-Channel Organic Field-Effect Transistors Based on Boron-Subphthalocyanine. *Mol. Cryst. Liq. Cryst.* **2007**, *462*, 3–9.
- (55) Pandey, R.; Gunawan, A. A.; Mkhoyan, K. A.; Holmes, R. J. Efficient Organic Photovoltaic Cells Based on Nanocrystalline Mixtures of Boron Subphthalocyanine Chloride and C₆₀. *Adv. Funct. Mater.* **2012**, *22*, 617–624.
- (56) Wang, Z. B.; Helander, M. G.; Greiner, M. T.; Qiu, J.; Lu, Z. H. Analysis of Charge-Injection Characteristics at Electrode-Organic Interfaces: Case Study of Transition-Metal Oxides. *Phys. Rev. B: Condens. Matter Mater. Phys.* **2009**, *80*, 235325.
- (57) Singh, M.; Mahajan, A.; Bedi, R. K.; Aswal, D. K. Dielectric Spectroscopic Studies of Boron Subphthalocyanine Chloride Thin Films. *Electron. Mater. Lett.* **2013**, *9*, 101–106.
- (58) Bassler, H. Charge Transport in Disordered Photoconductors. *Phys. Stat. Sol. B* **1993**, *175*, 15–56.
- (59) Pope, M.; Swenberg, C. E. *Electronic Processes in Organic Crystals and Polymers*, 2nd ed.; Oxford University Press: Oxford, U.K., 1999.
- (60) Pandey, A. K.; Dabos-Seignon, S.; Nunzi, J.-M. Pentacene: Ptcdi-C₁₃h₂₇ Molecular Blends Efficiently Harvest Light for Solar Cell Applications. *Appl. Phys. Lett.* **2006**, *89*, 113506.
- (61) Gonzalez-Rodriguez, D.; Torres, T.; Guldi, D. M.; Rivera, J.; Herranz, M. A.; Echegoyen, L. Subphthalocyanines: Tunable Molecular Scaffolds for Intramolecular Electron and Energy Transfer Processes. *J. Am. Chem. Soc.* **2004**, *126*, 6301–6313.

- (62) Wilson, M. W.; Rao, A.; Johnson, K.; Gelinas, S.; di Pietro, R.; Clark, J.; Friend, R. H. Temperature-Independent Singlet Exciton Fission in Tetracene. *J. Am. Chem. Soc.* **2013**, *135*, 16680–16688.
- (63) Peisert, H.; Knupfer, M.; Fink, J. Electronic Structure of Partially Fluorinated Copper Phthalocyanine (Cupcf4) and Its Interface to Au(100). *Surf. Sci.* **2002**, *515*, 491–498.
- (64) Yoon, M.-H.; Facchetti, A.; Stern, C. E.; Marks, T. J. Fluorocarbon-Modified Organic Semiconductors: Molecular Architecture, Electronic, and Crystal Structure Tuning of Arene- Versus Fluoroarene-Thiophene Oligomer Thin Film Properties. *J. Am. Chem. Soc.* **2006**, *128*, 5792–5801.
- (65) Cicerone, M. T.; Ediger, M. D. Photobleaching Technique for Measuring Ultraslow Reorientation near and Below the Glass Transition: Tetracene in O-Terphenyl. *J. Phys. Chem.* **1993**, *97*, 10489–10497.